RSC Advances

PAPER

View Article Online
View Journal | View Issue

Check for updates

Cite this: *RSC Adv.*, 2019, **9**, 1849

Mono and dual hetero-structured M@poly-1,2 diaminoanthraquinone (M = Pt, Pd and Pt–Pd) catalysts for the electrooxidation of small organic fuels in alkaline medium†

Abla Ahmed Hathoot,[a] Khalid Mahmoud Hassan,*[b] Asmaa Galal Ali,[a] Ahmed Said Shatla,[ac] Helmut Baltruschat[c] and Magdi Abdel-Azzem[a]

Oxidation of some small organic fuels such as methanol (MeOH), ethanol (EtOH) and ethylene glycol (EG) was carried out in an alkaline medium using palladium (Pd)–platinum (Pt) nanoparticles/poly1,2-diaminoanthraquinone/glassy carbon (p1,2-DAAQ/GC) catalyst electrodes. Pd and Pt were incorporated into the p1,2-DAAQ/GC electrode using the cyclic voltammetry (CV) technique. The obtained Pd/p1,2-DAAQ/GC, Pt/p1,2-DAAQ/GC, Pt/Pd/p1,2-DAAQ/GC and Pd/Pt/p1,2-DAAQ/GC nanocatalyst electrodes were characterized by scanning electron microscopy (SEM), energy dispersive X-ray spectroscopy (EDX) and CV methods. Real active surface area (A_{real}) achieved by carbon monoxide (CO) adsorption using differential electrochemical mass spectroscopy (DEMS) technique. The electrochemical activity was evaluated and normalized to A_{real} per metal loading mass. The electrocatalytic oxidation of the small organic fuels at the prepared nanocatalyst electrodes was studied in 1.0 M NaOH solutions by CV and chronoamperometric (CA) techniques. Pt/Pd/p1,2-DAAQ/GC nanocatalyst electrode exhibited enhanced catalytic activity, better durability and higher tolerance to carbon monoxide generated in the oxidation reaction when compared with the other three studied nanocatalysts. The present investigation suggests that the studied nanocatalysts can be successfully applied in direct oxidation of small organic fuels, especially MeOH.

Received 12th November 2018
Accepted 18th December 2018

DOI: 10.1039/c8ra09342c

rsc.li/rsc-advances

Open Access Article. Published on 15 January 2019. Downloaded on 9/23/2024 8:21:10 AM.
This article is licensed under a Creative Commons Attribution-NonCommercial 3.0 Unported Licence.

1. Introduction

The ever-increasing energy demand to satisfy the development of modern society and the growing concerns about environmental pollution as well as climate change have rendered it imperative to seek for alternatives of fossil fuels.[1] Fuel cells, which change chemical energy into electrical energy, are considered a great innovation because of their environmental friendliness and exceptional productivity. Direct fuel cells (DFCs) oxidize small organic fuels such as methanol (MeOH), ethanol (EtOH) and ethylene glycol (EG) for versatile applications.[2,3] DFCs possess important research features, namely, high vitality change proficiency, no contamination release and simple operation.[4,5] Although platinum (Pt) catalysts have been widely used in fuel cells, palladium (Pd)-based catalysts have become important in the recent years because they are inexpensive and have excellent catalytic activities toward different fuel molecules.[6,7] Moreover, it has been discovered that Pd has better toxic substance protection during the operation of fuel cells. Alloying Pt with another metal can improve alcohol oxidation kinetics significantly.[8,9] As indicated by the dual-function mechanism, blending Pt with Pd can give oxygen containing species at a lower potential and debilitate the bond quality of Pt–CO_{ads}. The negatively charged Pd is more effective in catalytic oxidation of organic fuels because it facilitates the removal of intermediate products such as $(CH_3COO–)_{ads}$ and $(CO)_{ads}$ and simultaneously prohibits the buildup of $(CO)_{ads}$ on the catalyst surface. The removal of intermediate species and simultaneous mitigation of the buildup may lead to a desirable complete oxidation of ethanol (*i.e.*, breakage of the C–C bond)[10] and advance the oxidation/expulsion of CO in the form of CO_2. Electrodeposition of Pd on various supports to improve catalytic activity has been utilized to prepare different catalysts.[11]

The activity of core–shell structured Au–PtPd/C and Au–Pt/C nanoparticles (NPs) was tested for the electrooxidation of methanol. Au–PtPd NPs showed higher activity than Au–Pt NPs due to their enhanced tolerance for methanol oxidation.[12] Three-dimensional (3D) cubic superstructures of PtPd nanosheets displayed improved catalytic activity and long-term

[a]*Electrochemistry Laboratory, Chemistry Department, Faculty of Science, Menoufia University, Shibin El-Kom 32511, Egypt*

[b]*Electrochemistry Research Laboratory, Physics and Mathematics Engineering Department, Faculty of Electronic Engineering, Menoufia University, Menouf 23952, Egypt. E-mail: drkhalidhassan73@gmail.com; Tel: +201001303945*

[c]*Institute of Physical and Theoretical Chemistry, Bonn University, D-53117 Bonn, Germany*

† Electronic supplementary information (ESI) available. See DOI: 10.1039/c8ra09342c

Open Access Article. Published on 15 January 2019. Downloaded on 9/23/2024 8:21:10 AM.
This article is licensed under a Creative Commons Attribution-NonCommercial 3.0 Unported Licence.

stability towards methanol oxidation compared with Pt/C, as reported by Zhou *et al.*[13]

Conducting polymers (CPs) as supporting materials not only offer high specific surface areas, but also enhance deposition possibility and impact the absorption of small organic fuels.[14] The choice of an appropriate CP is an essential factor that influences the efficacy of catalysis. Current studies demonstrate that CPs have excellent potential to improve the application of modified electrodes.[15] CPs have great manufacturing adaptability, stability, and ecofriendliness and can effectively act as a redox mediator.[15,16] Moreover, CPs have good stability and efficient surface areas for incorporation of metal nanoparticles (NPs) and for preventing their agglomeration during metal deposition.[15] The synergistic impact of metal NPs and polymer films enhances the efficacy for oxidation of fuel molecules, decreases catalyst poisoning and improves the stability of metal NPs.[15,17] The electrodeposition of metal NPs in the polymer films improves their tolerance towards CO_{ads} species produced during the oxidation process and is an economical and appropriate method.[18]

In a previous study, we prepared a number of modified catalyst electrodes.[19] The aim of the present study is to prepare mono and binary catalysts composed of Pt and Pd NPs with controlled deposition order on a polymer film. Herein, we report the synthesis of poly1,2-diaminoanthraqinone (p1,2-DAAQ) as a support for the deposition of Pt and/or Pd by the cyclic voltammetry (CV) technique on glassy carbon (GC) to prepare Pt/p1,2-DAAQ/GC, Pd/p1,2-DAAQ/GC, Pd/Pt/p1,2-DAAQ/GC and Pt/Pd/p1,2-DAAQ/GC nanocatalyst electrodes. The presence of two carbonyl groups in 1,2-DAAQ monomer can provide chelating centers, helping metal incorporation on the electrode surface compared with other polyaniline derivatives.[20] The resultant nanocatalyst electrodes were characterized by scanning electron microscopy (SEM), energy dispersive X-ray spectroscopy (EDX) and CV techniques. Electrochemically active surface area (ECSA) measurements were performed by the differential electrochemical mass spectroscopy (DEMS) technique. Furthermore, the stability of the prepared catalysts for alcohol oxidation in an alkaline medium was examined by chronoamperometry (CA).

2. Experimental

2.1. Materials

1,2-Diaminoanthraqinone (1,2-DAAQ) of analytical grade was obtained from Aldrich. Sulfuric acid (H_2SO_4 98%) (Merck), acetonitrile (99.9%) HPLC (LAB-SCAN), MeOH, EtOH, EG (ADWIC) (98%) and lithium perchlorate ($LiClO_4$) were used without additional purification. Sodium hydroxide (NaOH), palladium chloride ($PdCl_2$) and chloroplatinic acid hexahydrate ($H_2PtCl_6 \cdot 6H_2O$) were analytical grade chemicals. Diamond paste (presi) (2.0 μm) and distilled water were utilized.

2.2. Instruments

Electrochemical experiments were performed using a potentiostat Model BASi EPSILON. All electrochemical experiments were performed using an electrochemical cell with a conventional three-electrode system. A GC electrode (3 mm in diameter) was used as the working electrode and a platinum wire as an auxiliary electrode. All recorded potentials were with respect to the Ag/AgCl reference electrode except for ESA measurements, which were related to reversible hydrogen electrode (RHE), whereas film formation was related to the Ag/Ag^+ reference electrode. SEM images and EDX measurements were performed utilizing QUANTA FEG 250 equipped with an energy dispersive X-ray spectrometer. DEMS measurements were performed using a quadrupole mass spectrometer (Balzer QMG-422) and dual thin layer flow through cell, in which a hydrophobic Teflon membrane formed an interface between the electrolyte and vacuum.[21]

2.3. Experimental procedure

2.3.1. Electrochemical preparation of p1,2-DAAQ/GC modified electrode. p1,2-DAAQ film formation was carried out using 1.0 mM 1,2-DAAQ monomer in acetonitrile containing 0.1 M $LiCLO_4$ at GC electrode and by utilizing the CV method. The electrode potential was swept at a rate of 0.5 V s^{-1} between 0.2 and 1.4 V for 15 cycles, as reported previously by our group.[22]

2.3.2. Metal nanoparticle electrodeposition. Monometallic Pd or Pd catalysts were prepared by immersing p1,2-DAAQ/GC modified electrodes in aqueous solution of 0.1 M H_2SO_4 containing 2.5 mM $PdCl_2$ or 2.5 mM H_2PtCl_2 in 0.1 M $HClO_4$. The CV technique was used to deposit the metal NPs by sweeping the potential in the range between −0.35 and +0.65 V at a sweep rate of 0.05 V s^{-1} for 25 cycles.[23] Finally, Pd/p1,2-DAAQ/GC and Pt/p1,2-DAAQ/GC catalyst electrodes were prepared. Bimetallic Pd/Pt or Pt/Pd was prepared similarly using the monometallic electrode (formed by 12 sweeps), followed by deposition of other MNPs (using 12 sweeps) to finally obtain Pd/Pt/p1,2-DAAQ/GC or Pt/Pd/p1,2-DAAQ/GC nanocatalyst electrodes. The results revealed that no electrochemical responses were identified at p1,2-DAAQ/GC modified electrode in 1.0 M NaOH in the potential between −0.9 V and +0.3 V, confirming the electroinactive behavior of polyaniline derivatives in a basic medium.[7] For each catalyst, the current was normalized to the active surface area.

2.3.3. Differential electrochemical mass spectroscopy (DEMS) technique. DEMS experiments were conducted by flowing CO in saturated 0.1 mM H_2SO_4 supporting electrolyte. CO was adsorbed at a constant electrode potential of 0.06 V. After the formation of a CO monolayer, the solution was exchanged with a pure supporting electrolyte 0.5 M H_2SO_4 under constant potential ($E = 0.06$ V) to maintain a solution free of CO. Then, the Faradaic and ionic currents were recorded during the positive potential sweep. Coverages of adsorbed CO formed either from the CO-saturated electrolyte or from ethanol were calculated using the amount of CO_2 formed during oxidation in the supporting electrolyte to elucidate electrode surface coverage.[21]

3. Results and discussion

3.1. Characterization of the prepared catalyst electrodes

3.1.1. Electrocatalytic activity. Polymer (p1,2-DAAQ/GC) in an alkaline medium showed no activity. The electroactivities of

 This journal is © The Royal Society of Chemistry 2019

Open Access Article. Published on 15 January 2019. Downloaded on 9/23/2024 8:21:10 AM.
This article is licensed under a Creative Commons Attribution-NonCommercial 3.0 Unported Licence.

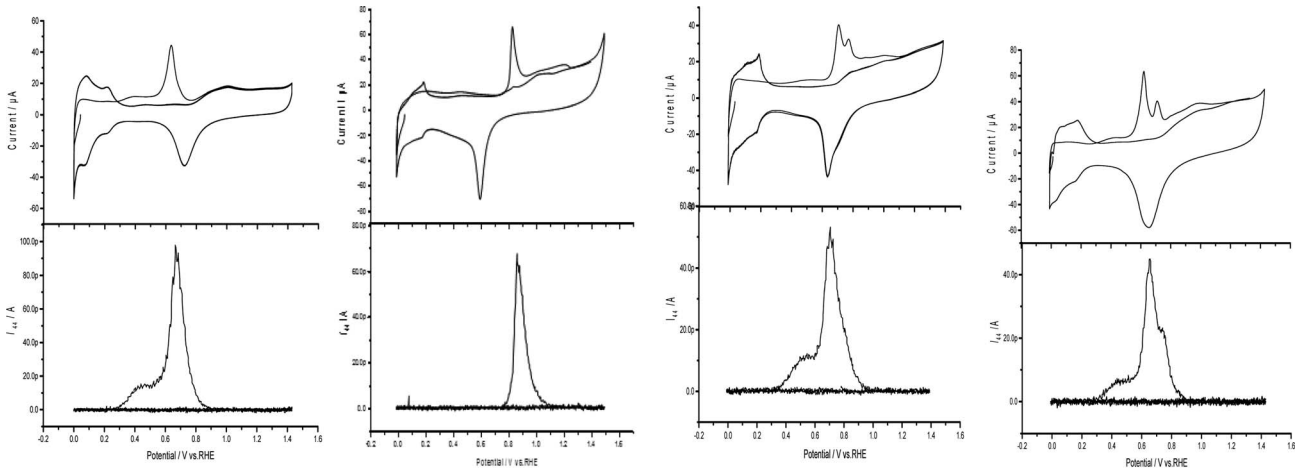

Fig. 1 Faradic and corresponding ion currents of CO_2 ($m/z = 44$) recoded at the same time throughout the electrooxidation of CO_{ads} at (A) Pd/p1,2-DAAQ/GC, (B) Pt/p1,2-DAAQ/GC, (C) Pd/Pt/p1,2-DAAQ/GC and (D) Pt/Pd/p1,2-DAAQ/GC catalyst electrodes in 0.5 M H_2SO_4.

Pd/p1,2-DAAQ/GC, Pt/p1,2-DAAQ/GC, Pt/Pd/p1,2-DAAQ/GC and Pd/Pt/p1,2-DAAQ/GC were examined in an alkaline medium in the absence of small organic fuels (Fig. S1†). The electrochemical redox responses of the nanocatalyst electrodes were different. Hydrogen adsorption/desorption was observed in the first region (around −0.85 V)[24] together with oxide formation/reduction in the second region in the potential range between −0.7 V and +0.4 V, in which metal oxide was formed in the forward scan. The single cathodic peak (initiating at −0.5 V for each electrode) largely belongs to the reduction of the formed metal oxide in the positive scan, with some minor contribution of reduction of dissolved oxygen.[25] Peaks in anodic and cathodic scans observed for all nanocatalyst electrodes revealed the signatures of the loaded Pd and Pt nanocatalysts on p1,2-DAAQ layer,[26] as illustrated by the real surface area (A_{real}).

A_{real} measurements of Pd/p1,2-DAAQ/GC, Pt/p1,2-DAAQ/GC, Pd/Pt/p1,2-DAAQ/GC and Pt/Pd/p1,2-DAAQ/GC nanocatalyst electrodes were achieved by the DEMS technique (*cf.* Experimental), as demonstrated in Fig. 1(A–D) (lower parts). Anodic oxidation peaks appeared at 0.88 V for Pt/p1,2-DAAQ/GC (Fig. 1B (upper part)) and at 0.66, 0.75 and 0.6 V for the other three nanocatalyst electrodes (Fig. 1A, C and D (upper parts), respectively), which were ascribed to the combined influence of oxidation of CO_{ads} and partial surface oxidation of Pt or Pd to metal oxides (PtO and PdO). Cathodic reduction peaks appeared at the reverse scan at 0.74, 0.60, 0.70 and 0.66 V for Pd/p1,2-DAAQ/GC, Pt/p1,2-DAAQ/GC, Pd/Pt/p1,2-DAAQ/GC and Pt/Pd/p1,2-DAAQ/GC catalyst electrodes, respectively, in 0.5 M H_2SO_4 at a sweep rate of 0.01 V s^{-1} (Fig. 1A–D (upper parts)), which were ascribed to metal oxide reduction. Charges associated with metal oxide reduction were deducted from the anodic charges and the charge was equivalent to CO_{ads} oxidation.[27,28] The ionic signal for $m/z = 44$ in 0.5 M H_2SO_4 at a sweep rate of 0.01 V s^{-1} and flow rate of 5.0 μL s^{-1} was used for A_{real} calculations, according to the following eqn (1):

$$A_{real} = A^{i}_{co} = Q_{MS}/K \times F\Gamma_{M}, \quad (1)$$

Here, Q_{MS} is the charge of mass spectrum (ionic signal), F is the Faraday constant, Γ_M is the surface concentration of CO_{ads} monolayer (assuming Γ_M of 1.45 nmol cm^{-2} corresponding to 280 μC cm^{-2}) and K is the calibration constant measured by CO stripping on Pt polycrystalline at a scan rate of 10.0 mV s^{-1}.

The obtained A_{real} values of the nanocatalyst electrodes were 0.87, 0.74, 0.73 and 1.0 cm^2 for Pd/p1,2-DAAQ/GC, Pt/p1,2-DAAQ/GC, Pd/Pt/p1,2-DAAQ/GC and Pt/Pd/p1,2-DAAQ/GC modified electrodes, respectively (Table 1). The results revealed that Pt/Pd/p1,2-DAAQ/GC modified electrode exhibited the largest A_{real} value, whereas both Pt/p1,2-DAAQ/GC and Pt/Pd/p1,2-DAAQ/GC exhibited the lowest values. These results indicated the important role of the order of metal NP electrodeposition.

Current is generally normalized by the mass of the loaded metal to study the catalyst efficiency. Therefore, electrochemically active surface area (ECSA) is an essential parameter and it explains the number of electrochemically active sites related to the mass of deposited metal[29,30] according to eqn (2):

$$\mathrm{ECSA} = Q/sl \quad (2)$$

Here, Q is the coulombic charge of the metal oxide reduction peak, s is the proportionality constant that correlates charge with area (0.405 mC cm^{-2}) and l is the electrocatalyst loading (g m^{-2}). Metal loading and ECSA for Pd/p1,2-DAAQ/GC, Pt/p1,2-DAAQ/GC, Pd/Pt/p1,2-DAAQ/GC and Pt/Pd/p1,2-DAAQ/GC

Table 1 A_{real}, metal loading and electrochemically active surface areas of the studied nanocatalyst electrodes

Catalysts	A_{real} (cm^2)	Metal loading (g m^{-2})	ECSA (m^2 g^{-1})
Pd/p1,2-DAAQ/GC	0.87	0.63	4.03
Pt/p1,2-DAAQ/GC	0.74	1.01	3.95
Pd/Pt/p1,2-DAAQ/GC	0.73	1.66	4.23
Pt/Pd/p1,2-DAAQ/GC	1.00	1.56	5.28

Open Access Article. Published on 15 January 2019. Downloaded on 9/23/2024 8:21:10 AM.
This article is licensed under a Creative Commons Attribution-NonCommercial 3.0 Unported Licence.

electrodes were calculated and the results are listed in Table 1. These results indicate that the mass of the metal loaded onto the bimetallic nanocatalysts has the largest value, whereas the mass of the metal loaded onto the mono metallic one has the lowest value. On the other hand, ECSA of Pt/Pd/p1,2-DAAQ/GC nanocatalyst electrode has the largest value.

3.1.2. Scanning electron microscopy (SEM) and energy dispersive X-ray spectroscopy (EDX). SEM was applied to analyze the morphology of p1,2-DAAQ/GC modified electrode as well as those of Pd/p1,2-DAAQ/GC, Pt/p1,2-DAAQ/GC, Pt/Pd/p1,2-DAAQ/GC and Pd/Pt/p1,2-DAAQ/GC nanocatalyst electrodes (Fig. 2(A–E)). The surface morphology of the p1,2-DAAQ/GC modified electrode (Fig. 2A) revealed nanorods with a smooth surface. Fig. 2B shows the image of Pd NPs deposited on p1,2-DAAQ/GC electrode, in which Pt particles appear as white spherical spots with an average diameter of approximately 243.2 nm dispersed on the electrode surface. Fig. 2C shows the image of Pt NPs deposited on p1,2-DAAQ/GC electrode, which differ greatly from those shown in Fig. 2B, which indicates that Pt NPs were deposited on the polymer surface. The surface morphology of the film changed from nanorods to nanoparticles due to Pd or Pt nanoparticle deposition onto p1,2-DAAQ matrix, affecting the electrical properties of the resulting film and its morphology.[31]

Fig. 2(D and E) show images of both Pt/Pd/p1,2-DAAQ/GC and Pd/Pt/p1,2-DAAQ/GC electrodes, respectively, where the particle sizes have average diameters of 88.0 nm and 68.0 nm, respectively. These data show that p1,2-DAAQ/GC is essentially affected by the incorporation of Pt and Pd NPs into the p1,2-DAAQ structure. This structure gives a high number of accessible active sites, acting as a valuable support for the deposition of Pt–Pd NPs. The conducting polymer surprisingly improves the active surface area and increases the catalyst activity. Moreover, the presence of Pt–Pd NPs in the polymeric film was affirmed by EDX (Fig. S2†). EDX results demonstrated that both Pd and Pt NPs were dispersed in the p1,2-DAAQ film with percentages of 13.44% and 32.54% for Pd/p1,2-DAAQ/GC and Pt/p1,2-DAAQ/GC electrodes, respectively. Furthermore, in the binary mixture of Pd and Pt NPs, EDX results revealed the presence of both dispersed metal NPs with percentages of 7.32 and 3.55% (Pd and Pt) as well as 3.54 and 1.62% (Pt and Pd) for Pd/Pt/p1,2-DAAQ/GC and Pt/Pd/p1,2-DAAQ/GC electrodes, respectively. The NP size distribution histograms of the four catalysts were manually obtained from the SEM images with more than 250 particles. The average NP sizes of Pd/p1,2-DAN/GC, Pt/p1,2-DAN/GC, Pt/Pd/p1,2-DAAQ/GC and Pd/Pt/p1,2-DAN/GC were 92.47, 143.88, 278.0 and 113.51 nm, respectively, as presented in Fig. 2(B(b), C(c), D(d) and E(e)). The difference between Fig. 2B and C originates from the broad range of NP size distributions of Pd NPs and their tendency to aggregate or to form clumps, as reported in literature.[32]

3.2. Catalytic activity towards electro-oxidation of alcohols

In a preliminary experiment, bare electrodes (Pt, Au and GC) were tested in 0.1 M NaOH solution containing 0.3 M MeOH, 1.0 M EtOH or 0.5 M EG. In general, no voltammetric response was observed at bare GC electrode, which is desirable to avoid any overlapping. For this reason, GC electrode was applied as the bare electrode in this study. Direct oxidation reactions of 0.3 M MeOH investigated in 1.0 M NaOH solutions at Pt/p1,2-DAAQ/GC, Pd/p1,2-DAAQ/GC, Pd/Pt/p1,2-DAAQ/GC and Pt/Pd/p1,2DAAQ/GC nanocatalyst electrodes were studied to inspect the impact of the presence of metal NPs and the deposition

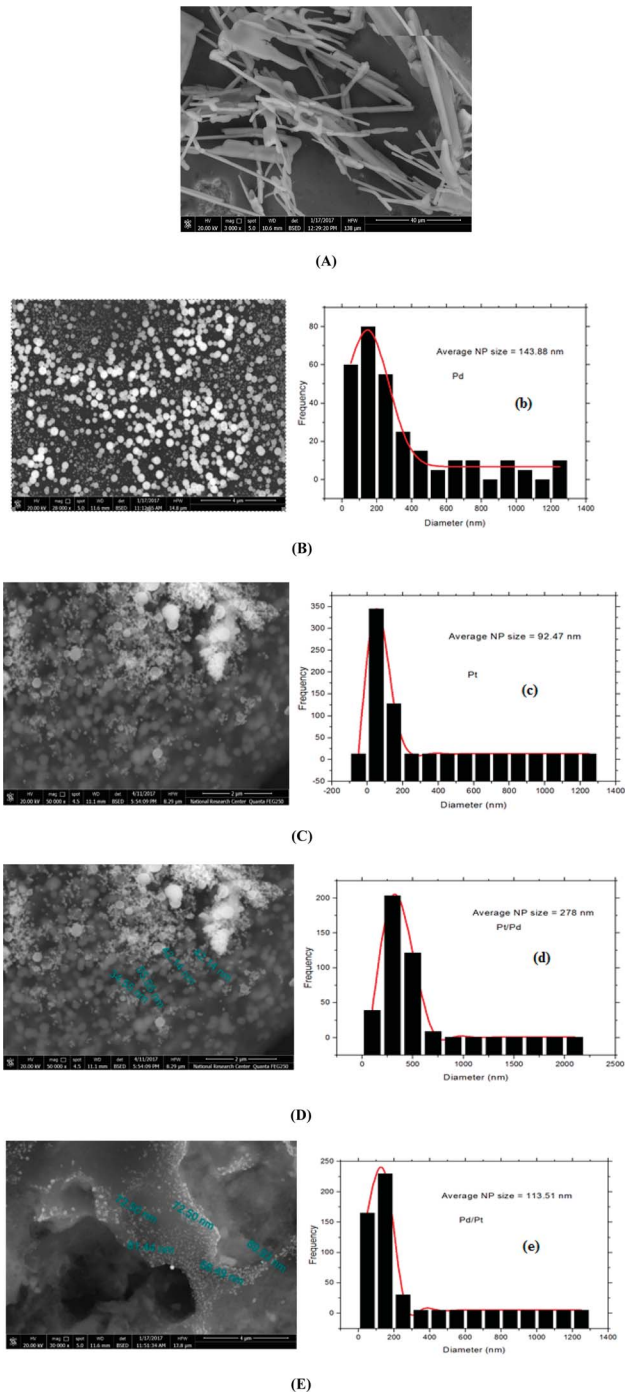

Fig. 2 SEM images of (A) p1,2-DAAQ/GC, (B) Pd/p1,2-DAAQ/GC, (C) Pt/p1,2-DAAQ/GC, (D) Pt/Pd/p1,2-DAAQ/GC and (E) Pd/Pt/p1,2-DAAQ/GC electrodes and the corresponding diameter distribution histograms of (B, b) Pd/p1,2-DAAQ/GC, (C, c) Pt/p1,2-DAAQ/GC, (D, d) Pt/Pd/p1,2-DAAQ/GC and (E, e) Pd/Pt/p1,2-DAAQ/GC electrodes.

This journal is © The Royal Society of Chemistry 2019

Open Access Article. Published on 15 January 2019. Downloaded on 9/23/2024 8:21:10 AM.
This article is licensed under a Creative Commons Attribution-NonCommercial 3.0 Unported Licence.

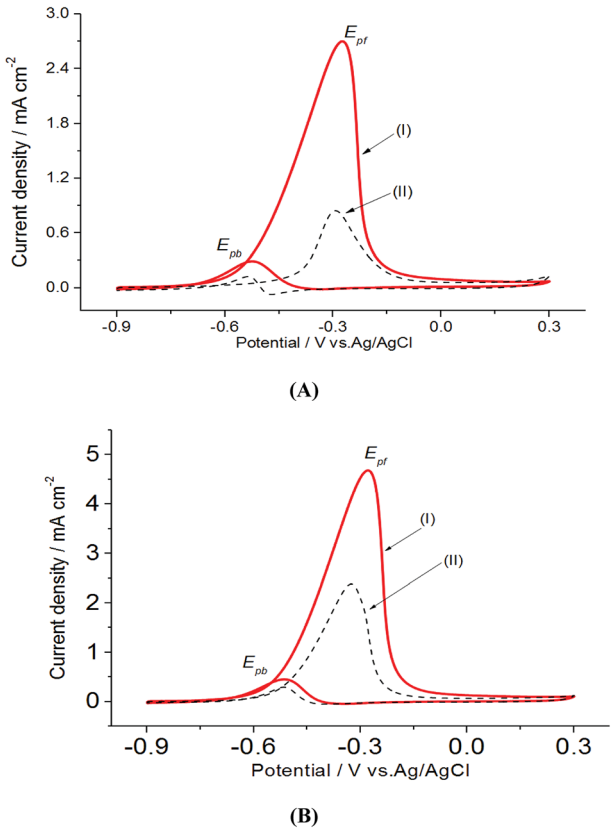

Fig. 3 Electrooxidation of 0.3 M MeOH in 1.0 M NaOH at a scan rate of 0.05 V s^{-1} for (A) single metal layer (I) Pt/p1,2-DAAQ/GC and (II) Pd/p1,2-DAAQ/GC and (B) bimetallic layer (I) Pt/Pd/p1,2-DAAQ/GC and (II) Pd/Pt/p1,2-DAAQ/GC nanocatalyst electrodes.

order of Pt and Pd on the catalytic activity of the prepared single and bimetallic nanocatalyst electrodes. As shown in Fig. 3(A and B), two oxidation peaks, *i.e.*, a forward oxidation peak (E_{pf}) and a backward peak (E_{pb}) were observed. These two peaks may be ascribed to the oxidation of EtOH and the intermediate species to CO_2.[33] The electrochemical data are presented in Table 2.

As seen in Table 2, the J_{pf}/J_{pb} ratio increased from 7.50 at Pd/p1,2-DAAQ/GC electrode to 10.35 at Pt/Pd/p1,2-DAAQ/GC electrode, indicating significant tolerance of this electrode against poisoning. This increase indicates improvement in catalytic activity. Alloying Pt with another metal improved alcohol oxidation kinetics significantly.[4,8,9] Thus, in the binary system, the study of Pt in an outer core and in an inner core was performed. The presence of Pt in the outer core improved the performance of the Pt/Pd/p1,2-DAAQ/GC electrode since incorporation of a second metal in Pd has been shown to improve liquid fuel oxidation kinetics significantly.[33] With respect to the dual-function and essential mechanism, a second metal can deliver oxygen-containing species at lesser potentials, reduce the bond strength of Pd–CO_{ads}, and facilitate oxidation of CO to CO_2 and its subsequent removal.[34] Moreover, the adsorption of intermediates produced from methanol oxidation, such as $(COH)_{ads}$, requires three neighboring platinum sites to be adsorbed; however, in the case of Pt/Pd/p1,2-DAAQ/GC, the presence of Pd NPs has a diluting effect and limits the presence of three adjacent Pt sites necessary for adsorption of the poisoning species.[35] Therefore, CO tolerance is significant at this electrode. On the other hand, in the case of Pd/Pt/p1,2-DAAQ/GC, Pd NPs are less active[36] towards methanol oxidation and therefore, their CO tolerance is small, leading to decreased CO poisoning and enhanced catalytic activity and durability toward MOR.[37]

Also, it was noticed that the forward peak current density at Pt/Pd/p1,2-DAAQ/GC electrode has a higher value compared with those of the other three catalysts. In general, the presence of p1,2-DAAQ film loaded with Pt, Pd or Pt/Pd (layer by layer) NPs provides catalytic enhancement for direct MeOH oxidation in terms of increasing oxidation current and favorable shift in the onset potential compared with commercial Pd/C (−0.38 V) and Pt/C (−0.52 V), as reported previously.[38]

On the other hand, electrooxidation of EtOH was examined in 1.0 M NaOH solutions at Pt/p1,2-DAAQ/GC, Pd/p1,2-DAAQ/GC, Pd/Pt/p1,2-DAAQ/GC and Pt/Pd/p1,2DAAQ/GC nanocatalyst electrodes, as illustrated in Fig. 4(A and B). One oxidation peak (E_{pf}) in the forward sweep generally ascribed to the oxidation of EtOH was observed. On the other hand, a reverse oxidation peak (E_{pb}) was noticed due to oxidation of the intermediate species.[6,23,39] The main challenge with ethanol is that the complete electrochemical oxidation per molecule involves complicated processes of 12 electrons and cleavage of a carbon–carbon (C–C) bond.[40] Pt-containing metallic catalysts can facilitate C–C bond cleavage.[41] It was found that electrochemical oxidation of EtOH greatly depends on the Pt content in the film matrix exposed to reaction conditions, where the percentage of Pt in case of Pt/Pd/p1,2-DAAQ/GC is higher than other catalysts; thus, the Pd/Pt/p1,2-DAAQ/GC electrode showed better tolerance. Table 3 shows the onset potential (E_{onset}) values, forward and backward peak potentials (E_{pf}, E_{pb}), anodic peak current densities for the forward and backward scans (J_{pf}, J_{pb}) and catalytic tolerances (J_{pf}/J_{pb}) for the electrooxidation of ethanol at the studied catalyst electrodes.

It is noticed that the J_{pf}/J_{pb} ratio increased from 0.27 at Pd/p1,2-DAAQ/GC to 3.3 at Pt/p1,2-DAAQ/GC, indicating significant tolerance of this electrode against poisoning. At the same time, Pt/Pd/p1,2-DAAQ/GC electrode showed the highest

Table 2 CV characteristics of the electrooxidation of 0.3 M MeOH at the studied nanocatalyst electrodes according to the first cycle

Catalyst	E^*_{onset}(V)	E^*_{pf}(V)	E^*_{pb}(V)	$J_{pf} \times 10^{-3}$ A cm^{-2}	$J_{pb} \times 10^{-3}$ A cm^{-2}	J_{pf}/J_{pb}
Pd/p1,2-DAAQ/GC	−0.62	−0.29	−0.53	0.75	0.10	7.50
Pt/p1,2-DAAQ/GC	−0.67	−0.28	−0.51	2.83	0.30	9.43
Pd/Pt/p1,2-DAAQ/GC	−0.65	−0.30	−0.51	2.40	0.36	6.66
Pt/Pd/p1,2-DAAQ/GC	−0.70	−0.28	−0.51	4.66	0.45	10.35

Open Access Article. Published on 15 January 2019. Downloaded on 9/23/2024 8:21:10 AM.
This article is licensed under a Creative Commons Attribution-NonCommercial 3.0 Unported Licence.

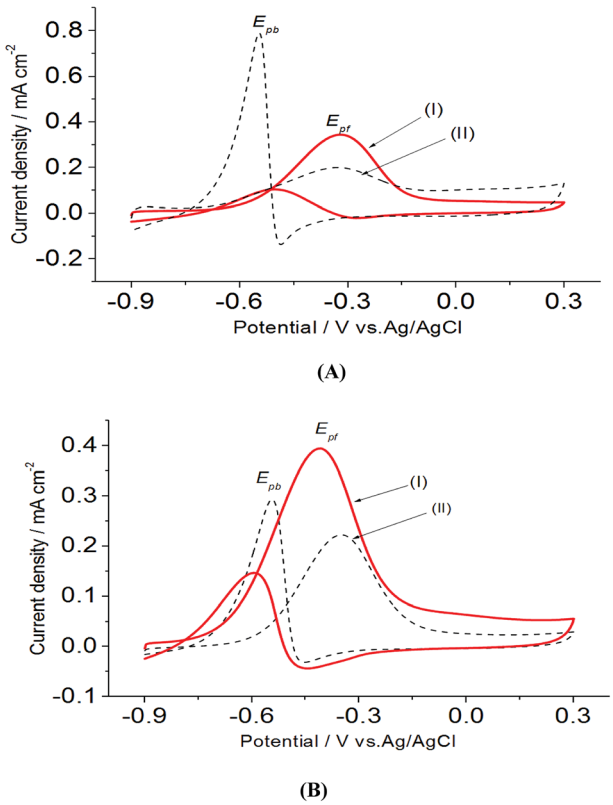

Fig. 4 Electrooxidation of 1.0 M EtOH in 1.0 M NaOH at a scan rate of 0.05 V s^{-1} for (A) single metal layer (I) Pt/p1,2-DAAQ/GC and (II) Pd/p1,2-DAAQ/GC and (B) bimetallic layer (I) Pt/Pd/p1,2-DAAQ/GC and (II) Pd/Pt/p1,2-DAAQ/GC nanocatalyst electrodes.

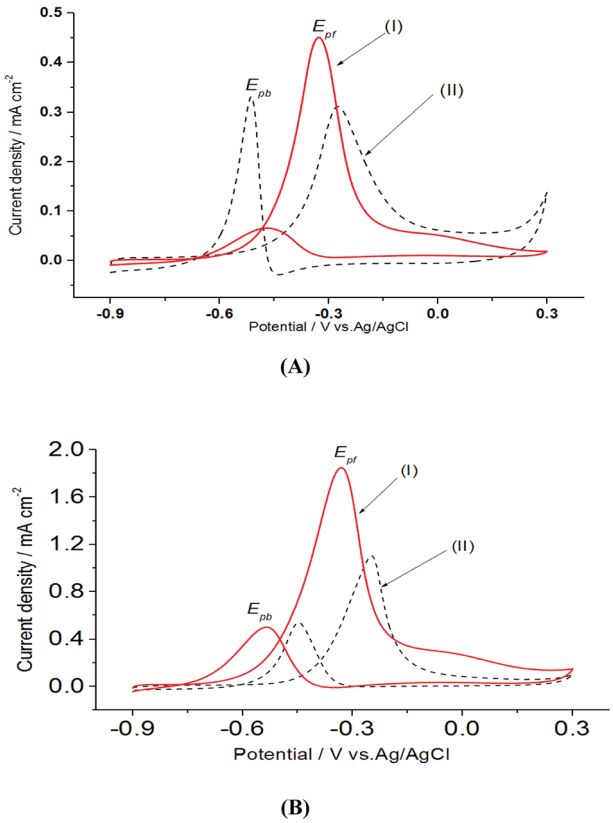

Fig. 5 Electrooxidation of 0.5 M EG in 1.0 M NaOH at a scan rate of 0.05 V s^{-1} for (A) single metal layer (I) Pt/p1,2-DAAQ/GC and (II) Pd/p1,2-DAAQ/GC and (B) bimetallic layer (I) Pt/Pd/p1,2-DAAQ/GC and (II) Pd/Pt/p1,2-DAAQ/GC nanocatalyst electrodes.

forward peak current density value and favorable onset potential shift, indicating catalytic enhancement towards ethanol oxidation. The values of ethanol E_{onset} were found to be −0.52 V and −0.51 V for Pd/C and Pt/C, respectively, as reported previously,[38] giving advantage to the studied catalysts.

Furthermore, cyclic voltammograms of the oxidation of EG at Pt/p1,2-DAAQ/GC, Pd/p1,2-DAAQ/GC, Pt/Pd/p1,2-DAAQ/GC and Pd/Pt/p1,2-DAAQ/GC electrodes studied in an alkaline medium showed two well-defined current peaks (Fig. 5(A and B)). The forward and the backward peaks correspond to the electrooxidation of EG and the intermediate species.[42] The onset potential, potential peak, current densities and J_{pf}/J_{pb} are listed in Table 4. Table 4 illustrates the onset potential (E_{onset}), forward and backward peak potentials (E_{pf}, E_{pb}), anodic peak currents for forward and backward scans (J_{pf} and J_{pb}) and catalytic tolerance (J_{pf}/J_{pb}) for the electrooxidation of EG at the studied catalyst electrodes.

Analysis of the previous data illustrated the importance of Pt and Pd NP deposition order. When we deposited Pd first, followed by the deposition of Pt, the formed Pt/Pd/p1,2-DAAAQ/GC nanocatalyst electrode showed satisfactory performance in alcohol oxidation with the highest peak current, I_{pf}, and a negative shift of the onset potential (around −0.7 V) (Tables 2–4) as a significant factor.[43] It was concluded that the catalytic tolerance of Pt/Pd/p1,2-DAAQ/GC nanocatalyst electrode in the electrooxidation of MeOH is the best. This might be related to the fact that MeOH is C1 compound, which can easily break in the presence of a high amount of Pt, as observed in the case of Pt/Pd/p1,2-DAAQ. On the other hand, the presence of Pd in Pd/Pt/p1,2-DAAQ/GC electrode (which is less active towards EtOH oxidation and EG oxidation reactions) decreased the electroactivity of the catalyst.

Mass electrochemical activities of each nanocatalyst were calculated from the amount of metal loading and the related

Table 3 CV characteristics of the electrooxidation of 1.0 M EtOH at the studied catalyst electrodes according to the first cycle

Catalyst	E^*_{onset}(V)	E^*_{pf}(V)	E^*_{pb}(V)	$J_{pf} \times 10^{-3}$ A cm^{-2}	$J_{pb} \times 10^{-3}$ A cm^{-2}	J_{pf}/J_{pb}
Pd/p1,2-DAAQ/GC	−0.68	−0.32	−0.54	0.21	0.78	0.27
Pt/p1,2-DAAQ/GC	−0.76	−0.32	−0.61	0.30	0.09	3.30
Pd/Pt/p1,2-DAAQ/GC	−0.70	−0.34	−0.54	0.23	0.29	0.75
Pt/Pd/p1,2-DAAQ/GC	−0.79	−0.42	−0.60	0.39	0.14	2.80

This journal is © The Royal Society of Chemistry 2019

Open Access Article. Published on 15 January 2019. Downloaded on 9/23/2024 8:21:10 AM.
This article is licensed under a Creative Commons Attribution-NonCommercial 3.0 Unported Licence.

Table 4 CV characteristics of the electrooxidation of 0.5 M EG at the studied catalyst electrodes according to first cycle

Catalyst	E_{onset} (V)	E_{pf} (V)	E_{pb} (V)	$J_{pf} \times 10^{-3}$ A cm^{-2}	$J_{pb} \times 10^{-3}$ A cm^{-2}	J_{pf}/J_{pb}
Pd/p1,2-DAAQ/GC	−0.46	−0.27	−0.49	0.31	0.33	0.94
Pt/p1,2-DAAQ/GC	−0.60	−0.31	−0.47	0.45	0.05	9.00
Pd/Pt/p1,2-DAAQ/GC	−0.53	−0.25	−0.44	1.10	0.53	2.07
Pt/Pd/p1,2-DAAQ/GC	−0.70	−0.34	−0.53	1.84	0.49	3.67

forward peak current densities are presented in Table 5. Therefore, Pt/Pd/p1,2-DAAAQ/GC nanocatalyst electrode was selected for the following electrochemical studies.

Based on the above results, the electroactivity of Pt/Pd/p1,2-DAAAQ/GC nanocatalyst electrode was examined for direct electrooxidation of MeOH, EtOH and EG by changing several parameters such as continuous cycling, scan rate, and alcohol and electrolyte concentrations.

3.3. Parameters affecting electrooxidation of the analyzed alcohols

To attain better electrocatalytic oxidation of the analyzed alcohols at Pt/Pd/p1,2-DAAAQ/GC nanocatalyst electrode, various parameters such as the effects of continuous cycling, scan rate, and alcohol and electrolyte concentrations were investigated.

3.3.1. Influence of permanent cycling. The applications of a catalyst depend significantly on its long-term cyclic stability. Therefore, it is imperative to study the impact of permanent cycling on the Pt/Pd/p1,2-DAAAQ/GC nanocatalyst electrodes in the presence of 0.3, 1.0 and 0.5 M MeOH, EtOH and EG, respectively. The relation between the anodic peak current density in the forward sweep and the number of cycles was recorded. It was noticed that at the beginning, increasing the number of cycles caused an increase in the current densities of the three alcohols, after which a steady state was observed. Currents densities began to decrease following 500, 250, and 400 sweeps for MeOH, EtOH and EG, respectively. The increase in the current density at the beginning could be due to the increase in diffusion within the catalyst layer. The accessible active sites of metal NPs increased with the diffusion of the alcohols. With increase in the cycle numbers, poisoning occurred and the structure of the nanocatalyst surface changed.[23,39]

3.3.2. Effect of scan rate. Kinetic characterizations of MeOH, EtOH and EG electrooxidation were performed at Pt/Pd/p1,2-DAAAQ/GC nanocatalyst electrodes by considering the influence of the sweep rates (Fig. S3†). The anodic peak current density in the forward scan is a function of the square root scan rate. The non-zero intercept can suggest the involvement of some types of surface interactions, suggesting that alcohol oxidation on the investigated catalysts is not a purely diffusion controlled process.[44]

It was concluded that diffusion controlled the catalytic reactions of the examined alcohols.[23,45] Also, cyclic voltammograms at various sweep rates demonstrated that the oxidation potential peaks in the forward sweep shifted to positive potentials with increase in scan rate. A linear correlation between E_p and $\log(V)$ indicated that the electrooxidation of the three alcohols is an irreversible electrochemical process.[46] The plots of J_{pf}/J_{pb} ratio *versus* scan rate indicate that the J_{pf}/J_{pb} ratio increases with increasing sweep rates. A higher J_{pf}/J_{pb} ratio indicates less nanocatalyst surface contamination with intermediates and an improvement in analyte oxidation.[23,47] Diffusion coefficient (D) was calculated for the studied alcohols according to the Randles–Sevcike equation,[48,49] yielding values of 7.4×10^{-8}, 3.34×10^{-8} and 1.7×10^{-8} for MeOH, EtOH and EG, respectively. These values are much lower than those reported earlier, indicating that the rate of the diffusion of alcohols to the electrode surface decreases at higher scan rates. The diffusion of penetrant through the polymer is greatly affected by the presence of impenetrable micro- and/or nano-particles located in the structure.[50,51]

3.3.3. Influence of alcohol and electrolyte concentrations. Pt/Pd/p1,2-DAAQ/GC electrode limitation for electrooxidation of various concentrations of the studied alcohols and its influence on the current density in the forward scan were assessed. The obtained data revealed that increasing the alcohol concentration increased the current densities in the forward sweep and achieved an almost steady state for concentrations greater than 1.6 M, 1.8 M and 1.4 M for MeOH, EtOH and EG, respectively. This may be because the reaction changes from a diffusion-

Table 5 Mass electrochemical activities of the studied nanocatalyst electrodes

		Methanol		Ethanol		Ethylene glycol	
Catalysts	Metal loading (g m^{-2})	J_{pf} (mA cm^{-2})	Mass electrochemical activity (A g^{-1})	J_{pf} (mA cm^{-2})	Mass electrochemical activity (A g^{-1})	J_{pf} (mA cm^{-2})	Mass electrochemical activity (A g^{-1})
Pd/p1,2-DAAQ/GC	0.63	0.75	11.90	0.21	3.30	0.31	4.92
Pt/p1,2-DAAQ/GC	1.01	2.83	28.01	0.30	2.90	0.45	4.40
Pd/Pt/p1,2-DAAQ/GC	1.66	2.40	14.40	0.23	1.38	1.10	6.60
Pt/Pd/p1,2-DAAQ/GC	1.56	4.66	29.87	0.39	2.50	1.84	11.79

Open Access Article. Published on 15 January 2019. Downloaded on 9/23/2024 8:21:10 AM.
This article is licensed under a Creative Commons Attribution-NonCommercial 3.0 Unported Licence.

controlled process at low concentrations to a reaction hindered by adsorbed intermediates at higher concentrations and lack of OH^- accessibility.[52] At higher alcohol concentrations, the surface of the nanocatalyst is covered by extra intermediate species. The dependence of alcohol oxidation peak potentials (E_p) on their concentrations was detected. The results show that upon increasing the alcohol concentrations, the E_p values shifted to positive potentials. This may be ascribed to the IR descent because of elevated oxidation current at high concentrations.[15]

The impact of different NaOH concentrations on the electrooxidation peak current densities of the studied alcohols at Pt/Pd/p-1,2DAAQ/GC nanocatalyst was examined by the CV technique. Increase in NaOH concentrations up to 1.0 M showed increase in the peak current densities, followed by a steady state in the range from 1.2 M to 1.4 M NaOH (figure not shown). Alcohol electrooxidation occurred due to higher accessibility and superior nanocatalyst surface coverage of OH^-.[23] Additional increment in the NaOH concentration resulted in decrease in the current density. At high NaOH concentrations, blocking of the Pt/Pd/p1,2-DAAQ/GC nanocatalyst electrode surface with OH^- ions occurred, hindering the adsorption of alcohol. Therefore, this OH^- blocking is extreme on metal NPs, whereas the intermediate coverage is poor, leading to decrease in current density.[23,53]

3.4. Possible elimination of nanocatalyst poisoning intermediates

The formation of catalyst-poisoning intermediate compounds, such as Pd or Pt–CO_{ads}, is the significant contributor to the decrease in the electrocatalytic activity during the alcohol oxidation reaction.[54] The development and dissolution of oxides formed on the nanocatalyst surface[23] were examined by expanding the final potentials to different values (from +0.4 to +0.9 V) (Fig. S4†). Expanding the final potential limits causes increase in the peak current densities in the forward scan.[42] In the reverse scan, the anodic peak current decreases.[55] The anodic peak potentials and peak current densities in the backward sweep changed with increasing the final potential limits. At low potential limits, sufficient metal NP oxides were not formed to oxidize the alcohols in the backward sweep. Increase in the final potential limits produced additional metal oxides, and the backward current density increased. Thus, it is clear that the final potential limits control the peak current densities of the forward J_{pf} and the reverse J_{pb} sweeps, increasing the tolerance of the nanocatalyst to intermediate species.[56] The influence of the nanocatalyst in eliminating poisonous intermediates was examined using the J_{pf}/J_{pb} ratio (Tables 1–3). It was found that the ratio increased from 10.0 to 122.0 (MeOH), 2.1 to 5.9 (EtOH) and 0.5 to 13.7 (EG) as the upper limit potential increased. It was noticed that E_{pf} showed similarity to E_{pb}, moving to low potential values with decrease in current densities. This demonstrates the continuing elimination of poisoning intermediates produced during the forward scan. Raising the potential limits in the forward scans increases metal oxide formation and decreases the peak potential E_{pf}.[42,57]

Finally, a comparison of the electrocatalytic activities of commercial Pt/C and Pt/Pd/p1,2-DAAQ/GC catalysts towards the oxidation of methanol, ethanol and ethylene glycol is displayed in Table 6. It was found that although Pt/Pd/p1,2-DAAQ/GC catalyst has lower current density compared with commercial Pt/C, it demonstrates higher tolerance and a negative onset potential shift. This can be ascribed to the role played by p1,2-DAAQ polymer film. The presence of the polymer not only offers a high specific surface area, but also enhances the deposition possibility and impacts the absorption of small organic fuels. The synergistic impact of metal NPs and polymer films enhances the efficacy of the oxidation of fuel molecules, decreases the catalyst poisoning and improves the stability of metal NPs, thus improving the tolerance against species produced during the oxidation process.

3.5. Chronoamperometry

Chronoamperometric study was carried out to better understand the electro-catalytic performance of the nanocatalyst electrode Pt/Pd/p1,2-DAAQ/GC. Fig. 6 shows the current–time transients, where the potentials are maintained at −0.28 V, −0.42 V, and −0.34 V for MeOH, EtOH and EG, respectively. By applying potential to the electrode, a steady decrease in currents was observed during the first few seconds, followed by the establishment of nearly fixed currents at longer times. The intermediate poisoning species formed during alcohol oxidation could be considered as the main factor for decreasing the current. Chronoamperometry study shows that the stability decreases in the order MeOH > EG > EtOH, which agrees with the above results.

Table 6 Comparison of electrocatalytic activities reported for Pt/C commercial catalyst and Pt/Pd/p1,2-DAAQ/GC electrode towards MeOH, EtOH and EG

Catalyst	Fuel	Concentration (M)	E^*_{onset}(V/Ag/AgCl)	E_{pf} (V/Ag/AgCl)	$J_{pf} \times 10^{-3}$ A cm^{-2}	Tolerance	Reference
Pt/C	MeOH	1.0 MeOH + 1.0 KOH	−0.55	−0.18	39	4.1	Ref. 38
Pt/Pd/p1,2-DAAQ/GC		1.0 MeOH + 1.0 NaOH	−0.70	−0.28	10.98	10.35	This work
Pt/C	EtOH	1.0 EtOH + 1.0 KOH	−0.55	−0.23	7	1.75	Ref. 38
Pt/Pd//p1,2-DAAQ/GC		1.0 EtOH + 1.0 NaOH	−0.79	−0.28	0.39	2.8	This work
Pt/C	EG	0.5 EG + 0.1 KOH	0.1	0.90	100	2	Ref. 58
Pt/Pd//p1,2-DAAQ/GC		0.5 EG + 0.1 NaOH	−0.70	−0.34	1.84	3.67	This work

This journal is © The Royal Society of Chemistry 2019

Open Access Article. Published on 15 January 2019. Downloaded on 9/23/2024 8:21:10 AM.
This article is licensed under a Creative Commons Attribution-NonCommercial 3.0 Unported Licence.

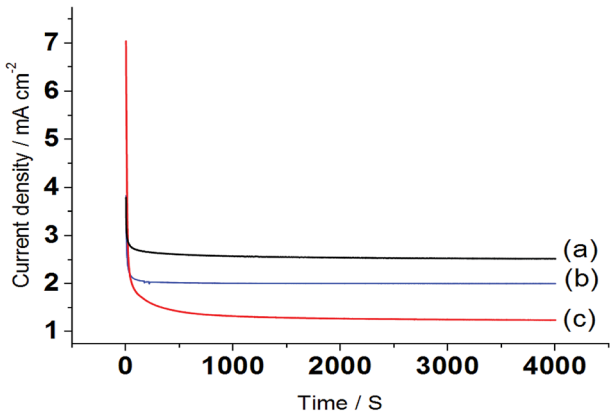

Fig. 6 Chronoamperograms for the electrooxidation of (a) 0.3 M MeOH, (b) 1.0 M EtOH and (c) 0.5 M EG in 1.0 M NaOH at Pt/Pd/p1,2-DAAQ/GC nanocatalyst electrode.

4. Conclusion

In the current study, we assessed the impact of p1,2-DAAQ/GC as a supporting material on the catalytic activity of Pd–Pt NP nanocatalyst for oxidation of MeOH, EtOH and EG. NPs were successfully deposited on p1,2-DAAQ/GC supports including Pt/p1,2-DAAQ/GC, Pd/p1,2-DAAQ/GC, Pd/Pt/p1,2-DAAQ/GC and Pt/Pd/p1,2-DAAQ/GC nanocatalyst electrodes by means of a simple and rapid process. Physicochemical characterization of the prepared nanocatalysts was performed by DEMS, SEM, EDX and electrochemical methods. Electrochemical examination demonstrated that the Pt/Pd/p1,2-DAAQ/GC nanocatalyst showed excellent catalytic activity for the oxidation of MeOH, EtOH and EG compared with other nanocatalysts. Therefore, Pt/Pd/p1,2-DAAQ/GC was chosen as the desired nanocatalyst electrode for our study. The influence of various factors on the oxidation of three alcohols was examined and improved. It was found that Pt/Pd/p1,2-DAAQ/GC electrocatalyst introduced high electroactivity and suitable and long-term cyclic stability, suggesting potential opportunities for its application as a suitable nanoelectrocatalyst. Furthermore, the catalytic tolerance of Pt/Pd/p1,2-DAAQ/GC nanocatalyst electrode in the electrooxidation of the studied alcohols decreased in the order MeOH > EG > EtOH, indicating that the Pt/Pd/p1,2-DAAQ/GC nanocatalyst electrode showed high catalytic activity in the electrooxidation of MeOH.

Conflicts of interest

There are no conflicts to declare.

Acknowledgements

The authors are appreciative of Alexander von Humboldt Foundation for financial funding of project no. 30260067.

References

1 D. D. Babu, Y. Huang, G. Anandhababu, M. A. Ghausi and Y. Wang, *ACS Appl. Mater. Interfaces*, 2017, **9**, 38621–38628.
2 H. Zhang, C. Hu, X. He, L. Hong, G. Du and Y. Zhang, *J. Power Sources*, 2011, **196**, 4499–4505.
3 A. Malolepszy, M. Mazurkiewicz, L. Stobinski, B. Lesiak, L. Kövér, J. Tóth, B. Mierzwa, A. Borodzinski, F. Nitze and T. Wågberg, *Int. J. Hydrogen Energy*, 2015, **40**, 16724–16733.
4 W. Xie, F. Zhang, Z. Wang, M. Yang, J. Xia, R. Gui and Y. Xia, *J. Electroanal. Chem.*, 2016, **761**, 55–61.
5 D. D. Babu, W. Wang, Y. Huang, J. Lv, Y. Wang and M. Wu, *Int. J. Hydrogen Energy*, 2018, **43**, 10351–10358.
6 Sh. Cao, W. Xu, Sh. Zhu, Y. Liang, Z. Li, Z. Cui, Y. Liang, Z. Li, X. Yang and A. Inouea, *J. Electrochem. Soc.*, 2016, **163**, E263–E271.
7 A. A. Hathoot, U. S. Yousef, A. S. Shatla and M. Abdel-Azzem, *Electrochim. Acta*, 2012, **85**, 531–537.
8 R. Ojani, J.-B. Raoof, M. Goli and R. Valiollahi, *J. Power Sources*, 2014, **264**, 76–82.
9 A. V. Tripković, K. D. Popović, B. N. Grgur, B. Blizanac, P. N. Ross and N. M. Marković, *Electrochim. Acta*, 2002, **47**, 3707–3714.
10 R. Jiang, D. T. Tran, J. P. McClure and D. Chu, *ACS Catal.*, 2014, **4**, 2577–2586.
11 F. Zhang, J. Chen, X. Zhang, W. Gao, R. Jin and N. Guan, *Catal. Today*, 2004, **93–95**, 645–650.
12 I.-S. Park, O.-H. Kim, J. W. Kim, B. Choi, Y.-H. Cho and Y.-E. Sung, *New J. Chem.*, 2015, **39**, 6034–6039.
13 L. N. Zhou, X. T. Zhang, Z. H. Wang, S. Guo and Y. J. Li, *Chem. Commun.*, 2016, **52**, 12737–12740.
14 G. Anandhababu, S. C. Abbas, J. Lv, K. Ding, Q. Liu, D. D. Babu, Y. Huang, J. Xie, M. Wu and Y. Wang, *Dalton Trans.*, 2017, **46**, 1803–1810.
15 J.-B. Raoof, S. R. Hosseini and S. Rezaee, *Electrochim. Acta*, 2014, **141**, 340–348.
16 E. Antolini and E. R. Gonzalez, *Appl. Catal., A*, 2009, **365**, 1–19.
17 W. Zhou, Y. Du, F. Ren, C. Wang, J. Xu and P. Yang, *Int. J. Hydrogen Energy*, 2010, **35**, 270–3279.
18 M. H. Pournaghi-Azar and B. Habibi, *J. Electroanal. Chem.*, 2007, **601**, 53–62.
19 K. M. Hassan, A. A. Hathoot, M. F. Abo oura and M. A. Azzem, *RSC Adv.*, 2018, **8**, 6346–6355.
20 S. Y. Yeh and C. M. Wang, *J. Electroanal. Chem.*, 2006, **592**, 131–138.
21 A. A. Abd-El-Latif, C. J. Bondue, S. Ernst, M. Hegemann, J. K. Kaul, M. Khodayari, E. Mostafa, A. Stefanova and H. Baltruschat, *TrAC, Trends Anal. Chem.*, 2015, **70**, 4–13.
22 K. M. Hassan, S. E. Gaber, M. F. Altahan and M. A. Azzem, *Electroanalysis*, 2018, **30**, 1155–1162.
23 B. Habibi and S. Mohammadyari, *Int. J. Hydrogen Energy*, 2015, **40**, 10833–10846.
24 R. Kannan, A. R. Kim and D. J. Yoo, *Chin. Sci. Bull.*, 2014, **59**, 3413–3419.
25 Z.-x. Cai, C.-c. Liu, G.-h. Wu, X.-m. Chen and X. Chen, *Electrochim. Acta*, 2013, **112**, 756–762.
26 X. Chen, G. Wu, J. Chen, X. Chen, Z. Xie and X. Wang, *J. Am. Chem. Soc.*, 2011, **133**, 3693–3695.
27 S. Dash and N. Munichandraiah, *Electrochim. Acta*, 2012, **80**, 68–76.

Open Access Article. Published on 15 January 2019. Downloaded on 9/23/2024 8:21:10 AM.
This article is licensed under a Creative Commons Attribution-NonCommercial 3.0 Unported Licence.

28 J. Solla-Gullón, A. Rodes, V. Montiel, A. Aldaz and J. Clavilier, *J. Electroanal. Chem.*, 2003, **554–555**, 273–284.
29 A. E. Fetohi, R. S. Amin, R. M. Abdel Hameed and K. M. El-Khatib, *Electrochim. Acta*, 2017, **242**, 187–201.
30 R. M. Abdel Hameed, *J. Colloid Interface Sci.*, 2017, **505**, 230–240.
31 I. Kanelidis and T. Kraus, *Beilstein J. Nanotechnol.*, 2017, **8**, 2625–2639.
32 J. Kao, K. Thorkelsson, P. Bai, B. J. Rancatore and T. Xu, *Chem. Soc. Rev.*, 2013, **42**, 2654–2678.
33 K. M. Hassan, A. A. Hathoot, R. Maher and M. Abdel Azzem, *RSC Adv.*, 2018, **8**, 15417–15426.
34 Y. Zhang, G. Chang, H. Shu, M. Oyama, X. Liu and Y. He, *J. Power Sources*, 2014, **262**, 279–285.
35 G. Yang, Y. Zhou, H. B. Pan, C. Zhu, S. Fu, C. M. Wai, D. Du, J. J. Zhu and Y. Lin, *Ultrason. Sonochem.*, 2016, **28**, 192–198.
36 G. Gökag, J. M. Leger and F. Hahn, *Z. Naturforsch., B: J. Chem. Sci.*, 2003, **58**, 423–432.
37 L. Liu, X.-X. Lin, Si-Y. Zou, A.-J. Wang, J.-R. Chen and J.-J. Feng, *Electrochim. Acta*, 2016, **187**, 576–583.
38 C. Xu, L. Cheng, P. Shen and Y. Liu, *Electrochem. Commun.*, 2007, **9**, 997–1001.
39 F. Jiang, Z. Yao, R. Yue, Y. Du, J. Xu, P. Yang and C. Wang, *Int. J. Hydrogen Energy*, 2012, **37**, 14085–14093.
40 C. Lamy, E. M. Belgsir and J.-M. Leager, *J. Appl. Electrochem.*, 2001, **31**, 799–809.
41 L. L. Carvalho, F. Colmati and A. A. Tanaka, *Int. J. Hydrogen Energy*, 2017, **42**, 16118–16126.
42 R. Kannan, A. R. Kim and D. J. Yoo, *J. Appl. Electrochem.*, 2014, **44**, 893–902.
43 X. Yang, Q. Yang, J. Xu and C.-S. Lee, *J. Mater. Chem.*, 2012, **22**, 8057–8062.
44 J. D. Lović, *J. Appl. Chem.*, 2017, **90**, 2039–2045.
45 V. Bambagioni, C. Bianchini, A. Marchionni, J. Filippi, F. Vizza, J. Teddy, P. Serp and M. Zhiani, *J. Power Sources*, 2009, **190**, 241–251.
46 S. Yang, X. Zhang, H. Mi and X. Ye, *J. Power Sources*, 2008, **175**, 26–32.
47 A. Chatterjee, M. Chatterjee, S. Ghosh and I. Basumallick, *Int. J. Nucl. Energy Sci. Technol.*, 2012, **2**, 123–133.
48 S. M. Azab and A. M. Fekry, *RSC Adv.*, 2017, **7**, 1118–1126.
49 A. M. Fekry, *Biosens. Bioelectron.*, 2017, **87**, 1065–1070.
50 L. L. Van Loon, H. C. Allen and B. E. Wyslouzil, *J. Phys. Chem. A*, 2008, **112**, 10758–10763.
51 A. Eyvazkhani and M. Karimi, *Proceedings of the International Conference on Textile Engineering*, Rasht, Iran, October 27–29, 2009.
52 T. Lopes, E. Antolini and E. Gonzalez, *Int. J. Hydrogen Energy*, 2008, **33**, 5563–5570.
53 Z. X. Liang, T. S. Zhao, J. B. Xu and L. D. Zhu, *Electrochim. Acta*, 2009, **54**, 2203–2208.
54 R. Manoharan and J. Prabhuram, *J. Power Sources*, 2001, **96**, 220–225.
55 Y. Yu, T. Wang, Y. Fu, W. Su and J. Hu, *Int. J. Hydrogen Energy*, 2014, **39**, 17617–17621.
56 Y. Zhao, L. Zhan, J. Tian, S. Nie and Z. Ning, *Electrochim. Acta*, 2011, **56**, 1967–1972.
57 X. Yang, X. Wang, G. Zhang, J. Zheng, T. Wang, X. Liu, C. Shu, L. Jiang and C. Wang, *Int. J. Hydrogen Energy*, 2012, **37**, 11167–11175.
58 L. Xin, Z. Zhang, J. Qi, D. Chadderdon and W. Li, *Appl. Catal., B*, 2012, **125**, 85–94.

This journal is © The Royal Society of Chemistry 2019